SPACE Conferences and Exposition
31 Aug-2 Sep 2015, Pasadena, California
AIAA SPACE 2015 Conference and Exposition

Shape Control of Tensegrity Structures

James V. Henrickson,* John Valasek†
Texas A&M University, College Station, TX, 77843, USA

Robert E. Skelton,‡
UC San Diego, La Jolla, CA, 92093, USA

Tensegrity is a relatively new approach to structural design that has seen great advances in recent years. The unique properties of tensegrity structures allow for the design of deployable and lightweight structures—a combination highly applicable in the context of space systems. This work focuses on a rigorous development of shape control for tensegrity structures. The equilibrium configuration of a tensegrity structure is contingent on the tensions in its tensile members. As such, it is possible to effectively change the shape of the structure by changing those tensions. In pursuit of shape control, this work develops and demonstrates a methodology that permits calculation of the tensions that drive a given tensegrity structure from some initial configuration to some specified desired configuration. Simulation results are presented for two simple tensegrity structures: a 2D cross and a 3D prism. Results show that the approach successfully achieves shape control for simple tensegrity structures.

I. Introduction

Tensegrity, or tensional integrity, approaches structural design by simplifying structures to networks of "bars" and "strings". More specifically, a tensegrity structure consists purely of members that are loaded in either pure compression (bars) or pure tension (strings). The design of these tensegrity structures focuses on identifying stable configurations that are resistant to disturbance, which causes the tensegrity design approach to effectively be a fusion of traditional structures, dynamics, and control theory. Because tensegrity systems can be designed with multiple equilibrium configurations based on changing applied string tensions, they are particularly well suited for situations in which deployable or adaptive structures are desirable.[1,2] Additionally, the design of these structures can be carried out in such a way that the system complexity is easily parameterized, allowing for minimum-mass optimization based on specified structural requirements.[3–5] This approach, yielding lightweight deployable structures, makes tensegrity systems highly applicable in the context of space systems.

With regard to applications in space, the development of tensegrity-based space structures and systems has become increasingly prominent in the literature. Furuya analyzes several approaches to deploying tensegrity masts,[6] Tibert rigorously details the design and analysis of deployable masts and reflector antennas,[7,8] Djouadi presents an application in the form of a tensegrity-based antenna,[9] Sultan, Corless, and Skelton explore the design of a tensegrity-based space telescope,[10] and Zhao, Li, and Zhao propose a deployable telescope specifically purposed for microsatellite applications.[11] As can be seen, tensegrity-based space applications have begun to appear in the literature. This is driven not only by the attractiveness of the minimum-mass properties that can be achieved by tensegrity systems, but also by the controllability of these structures—a trait particularly useful in the area of deployable and adaptive structures.

A formal method for tensegrity shape control is desirable, if not required, for true exploration of the possibilities of tensegrity-based deployable structures. While methods have been developed for describing

*Graduate Research Assistant, Vehicle Systems & Control Laboratory, Department of Aerospace Engineering, Student Member AIAA, james.henrickson@tamu.edu

†Professor and Director, Vehicle Systems & Control Laboratory, Department of Aerospace Engineering, Associate Fellow AIAA, valasek@tamu.edu

‡Professor, Mechanical and Aerospace Engineering, AIAA Fellow, bobskelton@ucsd.edu

the configurations and dynamics of these unique structures, the task of actively controlling the shape of these structures remains a largely open area of research. That said, some preliminary work has been conducted. Wijdeven and Jager have described and demonstrated a method for generating reference trajectories for tensegrity structure transformations.[12] Kanchanasaratool and Williamson approach the task of tensegrity control by solving for changes in the lengths of the structure's bars.[13] Indirectly working towards some degree of shape control, Paul, Valero-Cuevas, and Lipson demonstrate using tensegrity structures for robotic locomotion—the shape control here being driven by a genetic algorithm seeking to meet the desired translation goal for the structure.[14] Specifically seeking to address deployment of tensegrity structures, Sultan and Skelton develop a method based on identifying an equilibrium manifold for the specified structure and desired transformation, actuating by changing the rest-length of each string member.[1] Aldrich and Skelton investigate shape control with a focus on minimum-time optimization.[15] Wroldsen, de Oliveira, and Skelton explore a Lyapunov-based approach for control of tensegrity systems.[16,17]

The unique contribution of this work is the development of a general method of shape control for Class 1 tensegrity systems in which string tensions are dynamically solved for based on the error between the current and desired shape configurations of the structure. Rather than outputting a reference trajectory, this method outputs the string tension histories required for the desired transformation. Actuation is achieved by changing the tensions in string members, and these tensions are directly solved for.

This paper is organized as follows: In Section II, definitions are given for formally describing tensegrity structures—this includes their construction, their internal and external forces, and their dynamics. Section III details the process of rewriting tensegrity system dynamics in such a way that string tensions can later be "factored out" and solved. Section IV proceeds to outline the developed method of stating tensegrity shape objectives, reforms the system dynamics in terms of error between current and desired configuration, and describes how to solve for the tensions required for the desired transformation. Simulation results demonstrating the developed control method on various test cases are given in Section V, and conclusions and planned avenues of future work are given in Sections VI and VII, respectively.

II. Tensegrity Definitions and Dynamics

In a sense, tensegrity systems are relatively straightforward—the system is simply a collection of uniaxially-loaded rigid bars. Developing equations of motion for these simple members is fairly trivial. The complexity of the task, however, comes in the form of scalability. A full tensegrity system may consist of hundreds if not thousands of individual members; as such, any formal development of a dynamical model needs to easily scale from 1 to n members. The key to describing the dynamics of a tensegrity system, therefore, hinges on how one *represents* those dynamics. This section introduces and defines the fundamentals of tensegrity systems.

A. Structure Configuration Definitions

The starting point involves describing the positions of every node in the system. The nodes are identified as the ends of each bar in the system—as such, a (Class 1) system consisting of b bars will have $2b$ nodes. The position of the ith node is described with $\mathbf{n}_i$. The full description of the nodes in the system is typically stored in a node matrix N, a $3 \times n$ matrix with the ith column describing the position of the ith node.

$$N = \begin{bmatrix} \mathbf{n}_1 & \dots & \mathbf{n}_n \end{bmatrix} \in \Re^{3\times n} \tag{1}$$

The members of the system (the bars and strings) are defined with member vectors b_i and s_i that describe each member's orientation and length. These vectors are then stored in the bar and string matrices, B and S, in which the bth column of B describes the bth bar, and so on.

$$B = \begin{bmatrix} \mathbf{b}_1 & \dots & \mathbf{b}_b \end{bmatrix} \in \Re^{3\times b} \tag{2}$$

$$S = \begin{bmatrix} \mathbf{s}_1 & \dots & \mathbf{s}_s \end{bmatrix} \in \Re^{3\times s} \tag{3}$$

Because any given bar or string member can be described with a simple vector difference between the two nodes it connects, it is possible to express the bar and string matrices in terms of the node matrix by defining bar and string connectivity matrices for the system, C_b and C_s, respectively.

$$B = NC_b^T \tag{4}$$

$$S = NC_s^T \tag{5}$$

For a system with s strings, b bars, and n nodes, C_b is a $b \times n$ matrix, and C_s is a $s \times n$ matrix. Each row gives the connectivity of a specific bar or string. This is done by including a -1 and 1 in the two columns corresponding to the nodes that member connects, with zeros elsewhere.

B. Force Definitions

Finally, an expression needs to be found that gives the forces acting on every node in the system. Excluding the internal forces of the rigid bars, these forces are caused by strings connected to the nodes. As such, a string force density matrix $\hat{\gamma}$ is defined, where each force density γ_i describes the force in the ith string divided by the length of that string.

$$\hat{\gamma} = \begin{bmatrix} \gamma_1 & 0 & \dots & 0 \\ 0 & \gamma_2 & \dots & 0 \\ \vdots & \vdots & \ddots & \vdots \\ 0 & 0 & \dots & \gamma_s \end{bmatrix} \tag{6}$$

$$\gamma_i = \frac{\text{force in string } s_i}{\|s_i\|} \tag{7}$$

Note that the hat operator here indicates the diagonalization of a vector—the vector in this case being the vector containing each of the scalar γ values. This operator is similarly used in a later section in describing bar masses and member lengths.

A force matrix F is then defined such that the ith column $\mathbf{f}_i$ describes the sum of the forces acting on the ith node. To account for external forces applied to the nodes, an external force matrix W is similarly defined, where the ith column $\mathbf{w}_i$ describes the sum of *external* forces applied to the ith node. Having defined string tensions and external forces, an expression for the force matrix can then be derived. The full derivation of this expression is excluded here, but it can be found in the literature.[4,18]

$$F = \begin{bmatrix} \mathbf{f}_1 & \dots & \mathbf{f}_n \end{bmatrix} \in \Re^{3\times n} \tag{8}$$

$$W = \begin{bmatrix} \mathbf{w}_1 & \dots & \mathbf{w}_n \end{bmatrix} \in \Re^{3\times n} \tag{9}$$

$$F = W - NC_s^T \hat{\gamma} C_s \tag{10}$$

Note that the definitions and subsequent development here assume a Class 1 tensegrity system in which there is only a single bar connected to any given node in the system. Further elaboration on these definitions can be found in.[4]

C. Tensegrity Matrix Dynamics

Deriving equations of motion for a single rigid bar within a given tensegrity structure is simple. Deriving these equations of motion for *every* bar in a system and succinctly describing these dynamics in a way that is easily scalable to a system with n members is a more complicated task. An in-depth description of this process is beyond the scope of this work but can be found in the literature.[18] The end result of the process is a simple matrix expression that fully describes the dynamics of any Class 1 tensegrity system:

$$\ddot{N}M + NK(\gamma) = W \tag{11}$$

where the following matrices have been defined.

$$M \equiv \frac{1}{12} C_b^T \hat{m} C_b + C_r^T \hat{m} C_r \tag{12}$$

$$K \equiv C_s^T \hat{\gamma} C_s - C_b^T \hat{\lambda} C_b \tag{13}$$

$$-\hat{\lambda} \equiv \lfloor \dot{B}^T \dot{B} \rfloor \hat{l}^{-2} \hat{m} \frac{1}{12} + \lfloor B^T F C_b^T \rfloor \hat{l}^{-2} \frac{1}{2} \tag{14}$$

Additionally note that the floor bracket operator returns the diagonal elements of the input matrix.

$$\lfloor A \rfloor = \begin{bmatrix} a_{1,1} & 0 & \dots & 0 \\ 0 & a_{2,2} & \dots & 0 \\ \vdots & \vdots & \ddots & \vdots \\ 0 & 0 & \dots & a_{n,n} \end{bmatrix} \tag{15}$$

III. X Coordinate Transform

Having now identified expressions for describing the connectivity, initial configuration, and motion of Class 1 tensegrity systems, the goal is to solve for the strains in the tensile members $\hat{\gamma}$ that drive the structure into some desired shape. Note that in the dynamics expression (Equation 11), $\hat{\gamma}$ is solely present in the K term. Additionally note that in the definition of this term (Equation 45), $\hat{\gamma}$ appears both explicitly and implicitly, as it contributes to $\hat{\lambda}$ by way of F, which is defined in Equation 10. To facilitate the algebra required to solve for $\hat{\gamma}$, a change of coordinates is performed.

A. X Matrix Definition

To start the transformation, the X matrix is defined as the product of the N and M matrices. Because the intent is to express the matrix dynamics in terms of this X matrix, an expression for N in terms of X can then be easily found. Additionally, because the M matrix is solely a function of the tensegrity structure's connectivity, it is constant. This allows one to further identify the first and second derivatives of the X matrix in terms of N.

$$X = NM \longrightarrow N = XM^{-1} \tag{16}$$

$$\dot{X} = \dot{N}M \longrightarrow \dot{N} = \dot{X}M^{-1} \tag{17}$$

$$\ddot{X} = \ddot{N}M \longrightarrow \ddot{N} = \ddot{X}M^{-1} \tag{18}$$

B. Conversion of Matrix Dynamics

Using these expressions, which allow for conversion between the N and X, it is possible to completely re-express the matrix dynamics given in Section II in terms of X. The conversion of Equation 11 is straightforward.

$$\ddot{N}M + NK = W \longrightarrow \ddot{X} + XM^{-1}K = W \tag{19}$$

Conversion of K, however, is a somewhat more challenging task. Starting with the $\hat{\lambda}$ term within K, we seek expressions for each element in the matrix (recall that $\hat{\lambda}$ is a diagonal matrix).

$$-\hat{\lambda} = \frac{1}{12}\lfloor \dot{B}^T \dot{B} \rfloor \hat{m} \hat{l}^{-2} + \frac{1}{2}\lfloor B^T F C_b^T \rfloor \hat{l}^{-2} \tag{20}$$

Focusing on the first term in the $\hat{\lambda}$ expression, a scalar equation for its ith diagonal element can be found. Note here that $\mathbf{e}_i$ is a vector of zeros except for the ith element, which is set to 1, where i corresponds to the ith member in the tensegrity structure.

$$\mathbf{e}_i^T \frac{1}{12}\lfloor \dot{B}^T \dot{B} \rfloor \hat{m} \hat{l}^{-2} \mathbf{e}_i = \frac{\|\dot{\mathbf{b}}_i\|^2 m_i}{12 l_i^2} \tag{21}$$

Before repeating this for the second term in $\hat{\lambda}$, it is necessary to first substitute in the expression previously given for F (Equation 10). Scalar expressions for the ith element can then be found.

$$\frac{1}{2}\lfloor B^T F C_b^T \rfloor \hat{l}^{-2} = \frac{1}{2}\lfloor B^T W C_b^T - B^T S \hat{\gamma} C_s C_b^T \rfloor \hat{l}^{-2} \tag{22}$$

$$\mathbf{e}_i^T \frac{1}{2}\lfloor B^T W C_b^T - B^T S \hat{\gamma} C_s C_b^T \rfloor \hat{l}^{-2} \mathbf{e}_i = \frac{1}{2 l_i^2}\mathbf{b}_i^T W C_b^T \mathbf{e}_i - \frac{1}{2 l_i^2}\mathbf{b}_i^T S \hat{\gamma} C_s C_b^T \mathbf{e}_i \tag{23}$$

The intent now is to factor out γ. This can be done by taking into account that, in general, $\hat{\mathbf{x}}\mathbf{y} = \hat{\mathbf{y}}\mathbf{x}$, where $\mathbf{x}$ and $\mathbf{y}$ are vectors, and the hat operator forms a diagonal matrix of the elements in the vector. Applying this to the final term of Equation 23 allows one to perform the following algebraic manipulation:

$$\hat{\gamma} C_s C_b^T \mathbf{e}_i = (C_s C_b^T \mathbf{e}_i)^{\wedge} \gamma \tag{24}$$

$$\frac{1}{2 l_i^2}\mathbf{b}_i^T S \hat{\gamma} C_s C_b^T \mathbf{e}_i = \frac{1}{2 l_i^2}\mathbf{b}_i^T S (C_s C_b^T \mathbf{e}_i)^{\wedge} \gamma \tag{25}$$

$$\mathbf{e}_i^T \frac{1}{2}\lfloor B^T W C_b^T - B^T S \hat{\gamma} C_s C_b^T \rfloor \hat{l}^{-2} \mathbf{e}_i = \frac{1}{2 l_i^2}\mathbf{b}_i^T W C_b^T \mathbf{e}_i - \frac{1}{2 l_i^2}\mathbf{b}_i^T S (C_s C_b^T \mathbf{e}_i)^{\wedge} \gamma \tag{26}$$

A final scalar expression, therefore, for the ith member of $\hat{\lambda}$ is found to be

$$\lambda_i = \frac{\|\dot{\mathbf{b}}_i\|^2 m_i}{12 l_i^2} + \frac{1}{2 l_i^2}\mathbf{b}_i^T W C_b^T \mathbf{e}_i - \frac{1}{2 l_i^2}\mathbf{b}_i^T S C_s C_b^T \mathbf{e}_i \gamma_i \tag{27}$$

In this equation, γ shows up in a single term. For this reason, the equation for λ can be re-written in a cleaner fashion:

$$\lambda = -\Lambda\gamma - \tau \tag{28}$$

$$\tau_i = \frac{\|\dot{\mathbf{b}}_i\|^2 m_i}{12 l_i^2} + \frac{1}{2 l_i^2}\mathbf{b}_i^T W C_b^T \mathbf{e}_i \tag{29}$$

$$\Lambda_i = \frac{1}{2 l_i^2}\mathbf{b}_i^T S C_s C_b^T \mathbf{e}_i \tag{30}$$

Recall that the objective here is to rewrite the tensegrity dynamics in terms of the defined X matrix. At this stage, a scalar equation for the ith element of λ has been identified and rearranged to facilitate the later solving of γ. This expression, however, still needs to be rewritten in terms of the defined X matrix. Specifically, the following terms need to be expressed in terms of X: $\mathbf{b}_i^T$, $\|\dot{\mathbf{b}}_i\|$, and S. This is easily accomplished by recalling the definition of the bar and string matrices, B and S, in Equations 4 and 5.

$$B = NC_b^T \tag{31}$$
$$= XM^{-1}C_b^T \tag{32}$$
$$B^T = C_b M^{-1} X^T \tag{33}$$
$$\mathbf{b}_i^T = \mathbf{e}_i^T C_b M^{-1} X^T \tag{34}$$
$$\|\dot{\mathbf{b}}_i\|^2 = \|\mathbf{e}_i^T C_b M^{-1} \dot{X}^T\|^2 \tag{35}$$
$$\tag{36}$$
$$S = NC_s^T \tag{37}$$
$$= XM^{-1}C_s^T \tag{38}$$

By substituting these definitions into the derived λ equation, a final expression for λ in terms of X is found.

$$\lambda = -\Lambda\gamma - \tau \tag{39}$$
$$\tau_i = \frac{m_i}{12l_i^2} C_b M^{-1} \mathbf{e}_i^T \dot{X}^T \dot{X} \mathbf{e}_i M^{-1} C_b + \frac{1}{2l_i^2} (\mathbf{e}_i^T C_b M^{-1} X^T) W C_b^T \mathbf{e}_i \tag{40}$$
$$\Lambda_i = \frac{1}{2l_i^2} \mathbf{e}_i^T C_b M^{-1} X^T X M^{-1} C_s^T C_s C_b^T \mathbf{e}_i \tag{41}$$
$$\tag{42}$$

This, combined with Equations 19, 45, and 12 yield the full system dynamics in terms of X. For the reader's convenience, the full X system dynamics are given here:

$$\ddot{X} + XM^{-1}K = W \tag{43}$$
$$M \equiv \frac{1}{12} C_b^T \hat{m} C_b + C_r^T \hat{m} C_r \tag{44}$$
$$K \equiv C_s^T \hat{\gamma} C_s - C_b^T \hat{\lambda} C_b \tag{45}$$
$$\lambda = -\Lambda\gamma - \tau \tag{46}$$

IV. Control Law

The full dynamics for any Class 1 tensegrity system have been presented and fully rewritten in terms of a defined matrix X. With the goal of solving for tensions $\hat{\gamma}$ that drive the system from some initial shape to some desired shape, the expression for λ was algebraically manipulated to facilitate solving for γ. Before a final control law can be synthesized, however, it is first necessary to introduce the method of specifying the desired final shape of the given tensegrity structure.

A. Shape Objectives

In setting up a method of specifying shape objectives for a given tensegrity structure, a driving motivation is flexibility. It is desirable that the implemented method is capable of letting one describe a variety of shape objectives: moving a single node to a specific position, moving several nodes to some z-coordinate, moving all nodes to various specific positions, etc. The approach implemented for this purpose involves defining two matrices, L and R. L is a $j \times 3$ matrix of ones and zeros that specifies the "axes of interest" for the system nodes, where j is the number of "axes of interest". Similarly, R is an $n \times h$ matrix of ones and zeros that specifies which of those system nodes are "nodes of interest"—that is, which of the nodes are desired to be driven to specific coordinates—where n is the number of nodes in the structure and h is the total number of "nodes of interest". By multiplying LNR, one can therefore extract the current values of the

"node coordinates of interest" for the node configuration N. This $j \times h$ matrix is defined as Y_c, which can be rewritten in terms of the defined X matrix.

$$Y_c = LNR \tag{47}$$
$$= LXM^{-1}R \tag{48}$$

With a matrix expression that outputs the current values of the node coordinates of interest, one simply needs to construct a similar matrix containing the desired values for the node coordinates of interest, $\bar{Y}$. A matrix describing the error between the current and desired node coordinates of interest can then be simply found by subracting $\bar{Y}$ from Y_c.

$$Y = Y_c - \bar{Y} \tag{49}$$
$$= LXM^{-1}R - \bar{Y} \tag{50}$$

B. Error Dynamics

An expression for error between current and desired node positions has now been defined in terms of the X matrix. To achieve the desired shape control, this error needs to be driven to zero. More specifically, it is desired that the error matrix, in addition to its first and second time derivatives, all go to zero. This goal is expressed as follows, in which Ψ and Ω are gain matrices that can be used to tune the error dynamics:

$$\ddot{Y} + \Psi\dot{Y} + \Omega Y = 0 \tag{51}$$

Because $\bar{Y}$, M, L, and R are constant, the time derivatives of the error matrix are easily obtained:

$$Y = LXM^{-1}R - \bar{Y} \tag{52}$$
$$\dot{Y} = L\dot{X}M^{-1}R \tag{53}$$
$$\ddot{Y} = L\ddot{X}M^{-1}R \tag{54}$$

These can then be substituted back into the expression for the desired error dynamics (Equation 51).

$$L\ddot{X}M^{-1}R + \Psi L\dot{X}M^{-1}R + \Omega(LXM^{-1}R - \bar{Y}) = 0 \tag{55}$$

Recalling the system dynamics in terms of X from Section III (Equation 19), an expression for $\ddot{X}$ can be found and substituted into Equation 55.

$$\ddot{X} = W - XM^{-1}K \tag{56}$$
$$L(W - XM^{-1}K)M^{-1}R + \Psi L\dot{X}M^{-1}R + \Omega(LXM^{-1}R - \bar{Y}) = 0 \tag{57}$$

This can then be expanded and rearranged:

$$LXM^{-1}KM^{-1}R = LWM^{-1}R + \Psi L\dot{X}M^{-1}R + \Omega LXM^{-1}R - \Omega\bar{Y} \tag{58}$$

The left-hand term can be rewritten by substituting in the previously-defined expression for K:

$$LXM^{-1}KM^{-1}R = LXM^{-1}(C_s^T\hat{\gamma}C_s - C_b^T\hat{\lambda}C_b)M^{-1}R \tag{59}$$

The ith column of this left-hand term can then be algebraically manipulated such that the vector γ appears linearly.

$$LXM^{-1}KM^{-1}R\mathbf{e}_i = LXM^{-1}\big[C_s^T(C_sM^{-1}R\mathbf{e}_i)^\wedge\gamma - C_b^T(C_bM^{-1}R\mathbf{e}_i)^\wedge\lambda\big] \tag{60}$$

Recalling that $\lambda = -\Lambda\gamma - \tau$, Equation 60 can be rewritten and rearranged once again such that γ appears linearly in a single term.

$$LXM^{-1}KM^{-1}Re_i = LXM^{-1}\Big[\big[C_s^T(C_sM^{-1}R\mathbf{e}_i)^\wedge + C_b^T(C_bM^{-1}R\mathbf{e}_i)^\wedge\Lambda\big]\gamma + C_b^T(C_bM^{-1}R\mathbf{e}_i)^\wedge\tau\Big] \tag{61}$$

C. Solving for Tensions

Now having an expression for the error dynamics in which the tensions γ appear linearly in a single term, the remaining task is to solve for γ in a way that satisfies the desired error dynamics in which they are driven to zero. The ith column of the full error dynamics are given as follows:

$$\begin{aligned}\big[LWM^{-1}R + \Psi L\dot{X}M^{-1}R + \Omega(LXM^{-1}R - \bar{Y})\big]\mathbf{e}_i \\ = LXM^{-1}\Big[\big[C_s^T(C_sM^{-1}R\mathbf{e}_i)^\wedge + C_b^T(C_bM^{-1}R\mathbf{e}_i)^\wedge\Lambda\big]\gamma + C_b^T(C_bM^{-1}R\mathbf{e}_i)^\wedge\tau\Big]\end{aligned} \tag{62}$$

This can be expanded and rearranged to isolate the γ term on the right hand side of the equation:

$$\begin{aligned}\big[LWM^{-1}R + \Psi L\dot{X}M^{-1}R + \Omega(LXM^{-1}R - \bar{Y})\big]\mathbf{e}_i - LXM^{-1}C_b^T(C_bM^{-1}R\mathbf{e}_i)^\wedge\tau \\ = LXM^{-1}\big[C_s^T(C_sM^{-1}R\mathbf{e}_i)^\wedge + C_b^T(C_bM^{-1}R\mathbf{e}_i)^\wedge\Lambda\big]\gamma\end{aligned} \tag{63}$$

One can simplify this into $\mu = \Gamma\gamma$ with careful definitions of μ_i and Γ_i, in which μ is the stack of each μ_i matrix and Γ is similarly a stack of each Γ_i matrix.

$$\mu = \Gamma\gamma \tag{64}$$

$$\mu_i = \big[LWM^{-1}R + \Psi L\dot{X}M^{-1}R + \Omega(LXM^{-1}R - \bar{Y})\big]\mathbf{e}_i - LXM^{-1}C_b^T(C_bM^{-1}R\mathbf{e}_i)^\wedge\tau \tag{65}$$

$$\Gamma_i = LXM^{-1}\big[C_s^T(C_sM^{-1}R\mathbf{e}_i)^\wedge + C_b^T(C_bM^{-1}R\mathbf{e}_i)^\wedge\Lambda\big] \tag{66}$$

By doing so, γ can then be solved for at the current time-step with linear programming. Note that by alternatively solving with the pseudo-inverse of Γ, string tension constraints cannot be applied. That is, numerical results can and likely will include instances in which nodes are "pushed" with strings. By solving for γ with linear programming, however, one can enforce a constraint that all tensions values must be positive.

V. Simulation Results

In this section, simulation results demonstrating the developed control method are provided for both a simple 2D tensegrity cross and a 3D tensegrity triangular prism. For each, results are presented for cases in which tensions *are* constrained to positive values. These constrained cases are in-line with solutions that would yield physically realizable shape control of tensegrity structures.

A. 2D Cross

The 2D cross is a standard test case for testing tensegrity dynamics in two dimensions. It consists of two bars and four strings and is defined by the following connectivity and initial node matrices. The initial configuration of this system is shown in Figure 1. In this and all following figures, bar members are represented with black lines, and string members with red lines.

$$C = \begin{bmatrix} -1 & 1 & 0 & 0 \\ 0 & -1 & 1 & 0 \\ 0 & 0 & -1 & 1 \\ 1 & 0 & 0 & -1 \\ -1 & 0 & 1 & 0 \\ 0 & -1 & 0 & 1 \end{bmatrix}$$

$$N_0 = \begin{bmatrix} 1 & 0 & -1 & 0 \\ 0 & 1 & 0 & -1 \\ 0 & 0 & 0 & 0 \end{bmatrix}$$

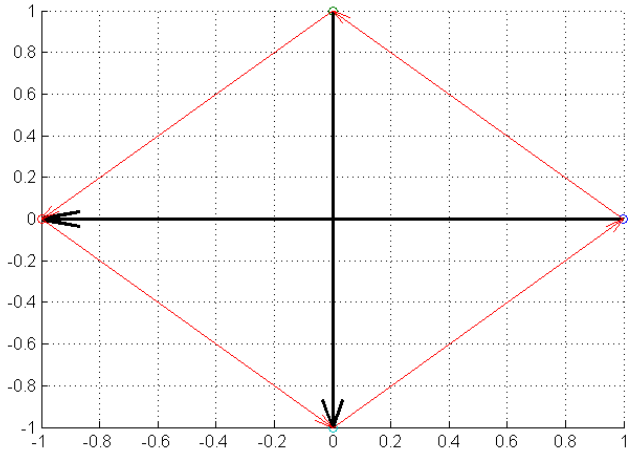

Figure 1. Initial configuration of 2D cross

Case 1: Node 1 to x = 0

The first 2D cross case attempts to drive node 1—initially at (1,0)—to a final position in which $x = 0$. The control tensions are solved in this and all following cases using MATLAB's 'lsqlin' function with a positivity constraint on γ. Additionally, in this case and all subsequent cases, the stabilizing coefficients Ψ and Ω are set equal to 1 unless otherwise specified.

$$L = \begin{bmatrix} 1 & 0 & 0 \end{bmatrix} \tag{67}$$

$$R = \begin{bmatrix} 1 & 0 & 0 & 0 \end{bmatrix}^T \tag{68}$$

$$\bar{Y} = 0 \tag{69}$$

A 6-image time-lapse of the resulting transformation is given in Figure 2, the node position history and final structure configurations are shown in Figure 3, and tension histories for the transformation are shown in Figure 4. From the time-lapse, it is evident here that node 1 can be driven to the desired position, but it cannot be held there. Rather than remaining at the origin, node 1 slowly shifts to the right until the end of the simulation. This is intuitive when looking at the final structure configuration—given that the

red lines are strings in tension, the final configuration is clearly unreachable and unstable without negative string tensions. Rather than relying on intuition, this can also be reasoned by considering the center of mass of the structure. Because no external forces are being applied to the structure, its center of mass must remain constant through any transformation driven solely by changing string tensions. The vertical bar must therefore be horizontally displaced the same amount as that of the horizontal bar. For the final configuration found that places node 1 at the origin, this requires the two bars to no longer be overlapping, which cannot be sustained with positive tensions.

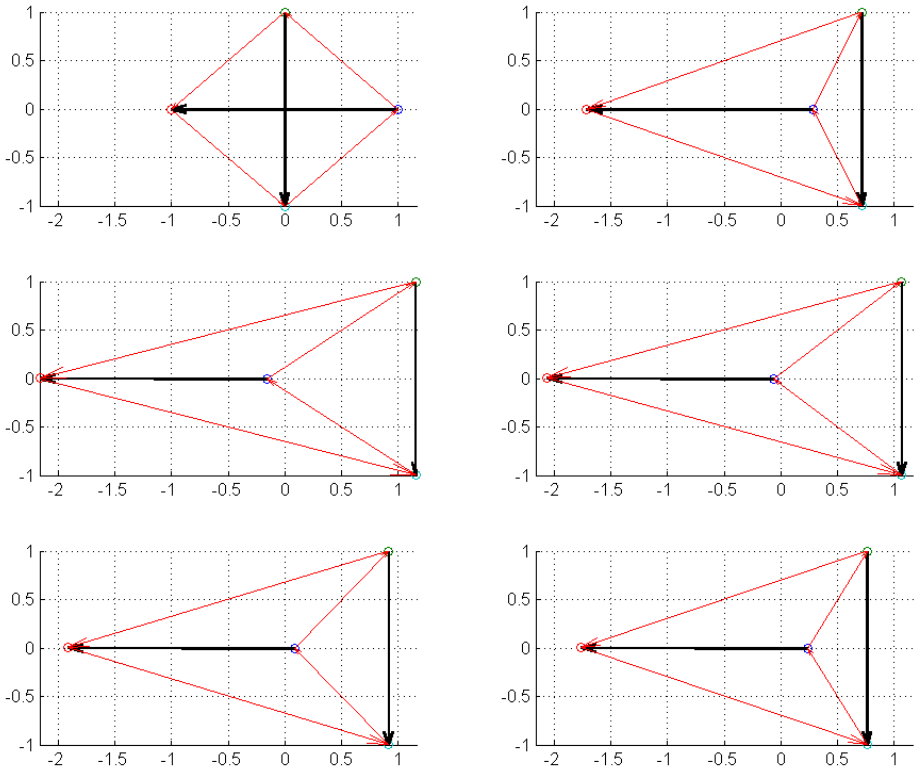

Figure 2. 2D cross transformation time-lapse for control case 1

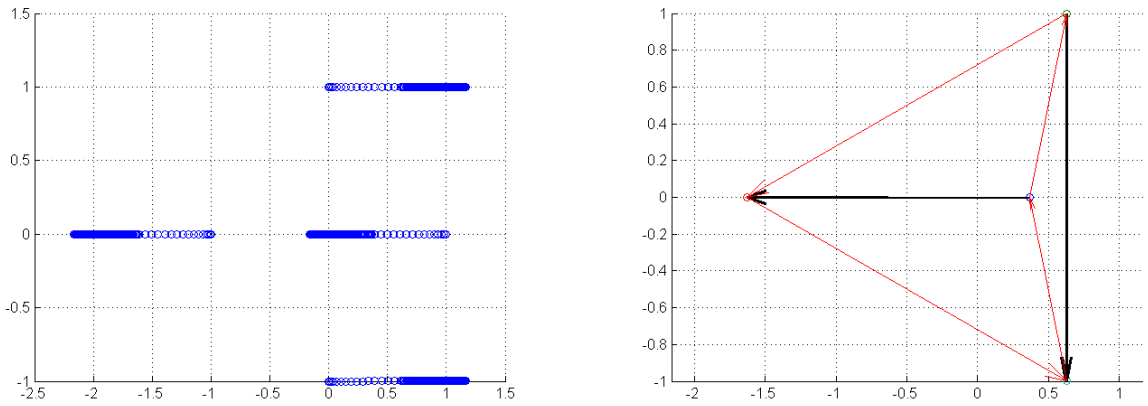

a. Node history b. Final member positions

Figure 3. 2D cross node history and final member position for control case 1

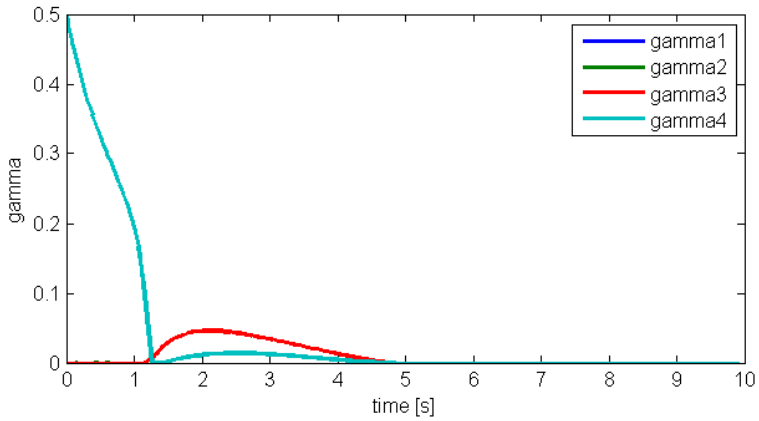

Figure 4. 2D cross tension history for control case 1

Case 2: Node 1 to x = 0.75

Based on the discussion of center of mass for the 2D cross, one would expect that there should exist some physically realizable transformation for this 2D cross as long as the bars overlap in the final configuration. To assess whether or not the control method is able to identify a solution that agrees with this, the following case aims to move node 1—initially at (1,0)—to a position in which $x = 0.75$.

$$L = \begin{bmatrix} 1 & 0 & 0 \end{bmatrix} \tag{70}$$

$$R = \begin{bmatrix} 1 & 0 & 0 & 0 \end{bmatrix}^T \tag{71}$$

$$\bar{Y} = 0.75 \tag{72}$$

A 6-image time-lapse of the resulting transformation is given in Figure 5, the node position history and final structure configurations are shown in Figure 6, and tension histories for the transformation are shown in Figure 7. The results shown here are as expected—a solution was found that achieves the desired transformation while yielding a final equilibrium configuration that is physically realizable with positive tension values.

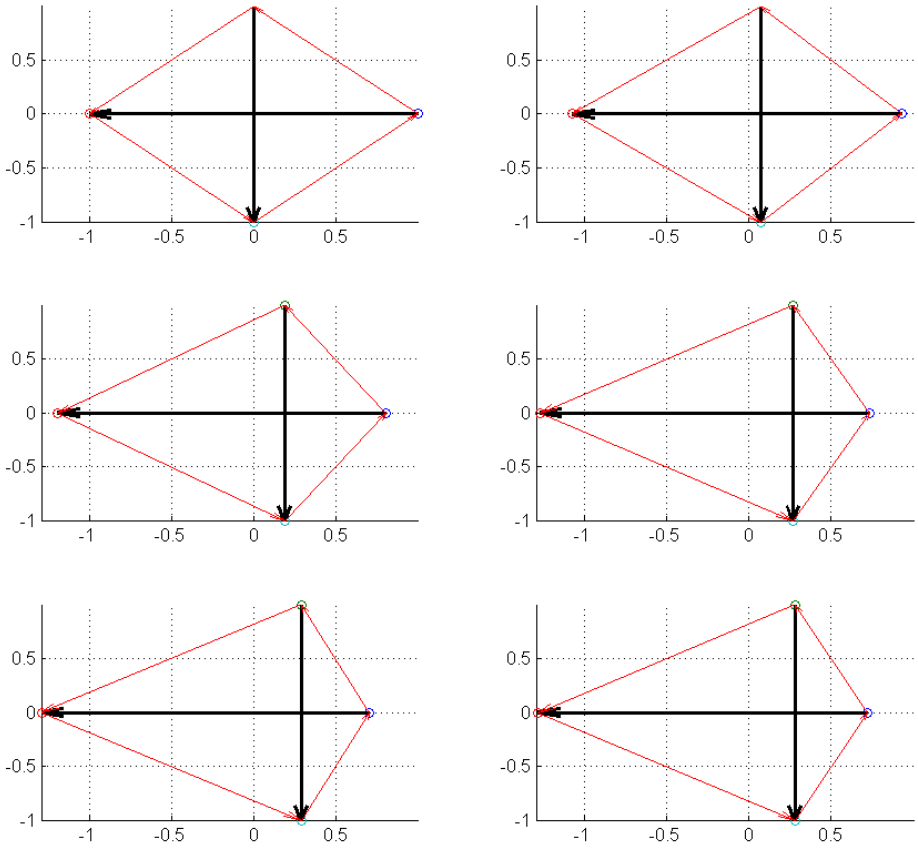

Figure 5. 2D cross transformation time-lapse for control case 2

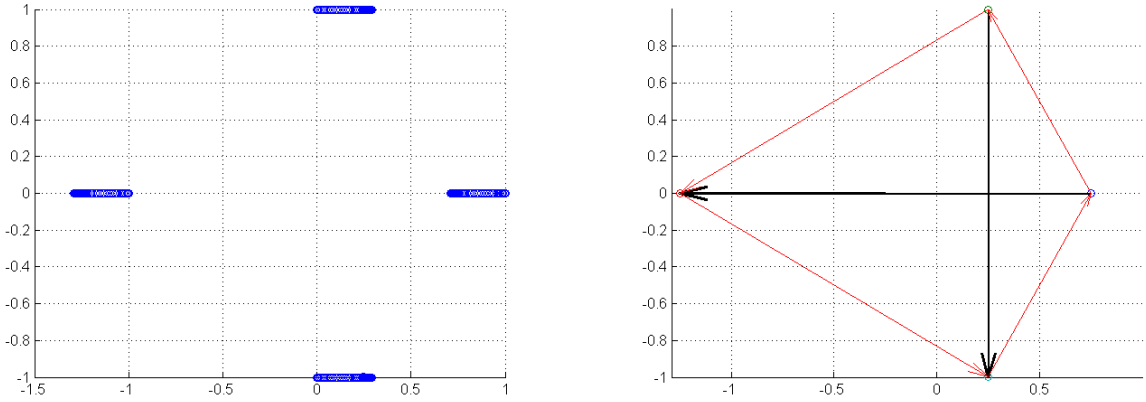

a. Node history

b. Final member positions

Figure 6. 2D cross node history and final member position for control case 2

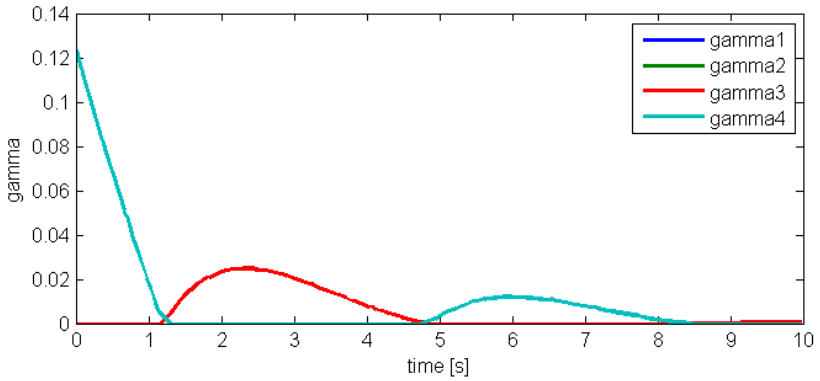

Figure 7. 2D cross tension history for control case 2

Case 3: Nodes 1 and 2 to (0.5,0.5) To illustrate multiple nodes simultaneously, the third case for the 2D cross involves driving nodes 1 and 2—initially at positions (1,0) and (0,1), respectively—to a final position of (0.5,0.5). Note that in this case, the Ψ stabilizing coefficient was changed from 1 to 3 due to solution convergence issues with a configuration that occurs with excessive overshoot. Note that, in terms of tuning, increasing Ψ slows down control response, yielding less overshoot but slower rise time. Increasing Ω has the opposite effect—increasing overshoot and yielding faster rise times. Problems with solution convergence are not entirely unexpected. It stands to reason that there exist system configurations in which shape objectives are simply not achievable when including tension positivity requirements. The corresponding shape objective matrices are given as follows:

$$L = \begin{bmatrix} 1 & 0 & 0 \\ 0 & 1 & 0 \end{bmatrix} \tag{73}$$

$$R = \begin{bmatrix} 1 & 0 \\ 0 & 1 \\ 0 & 0 \\ 0 & 0 \end{bmatrix} \tag{74}$$

$$\bar{Y} = \begin{bmatrix} 0.5 & 0.5 \\ 0.5 & -.5 \end{bmatrix} \tag{75}$$

A 6-image time-lapse of the resulting transformation is given in Figure 8, the node position history and final structure configurations are shown in Figure 9, and tension histories for the transformation are shown in Figure 10. The transformation solution here is able to achieve the desired final configuration.

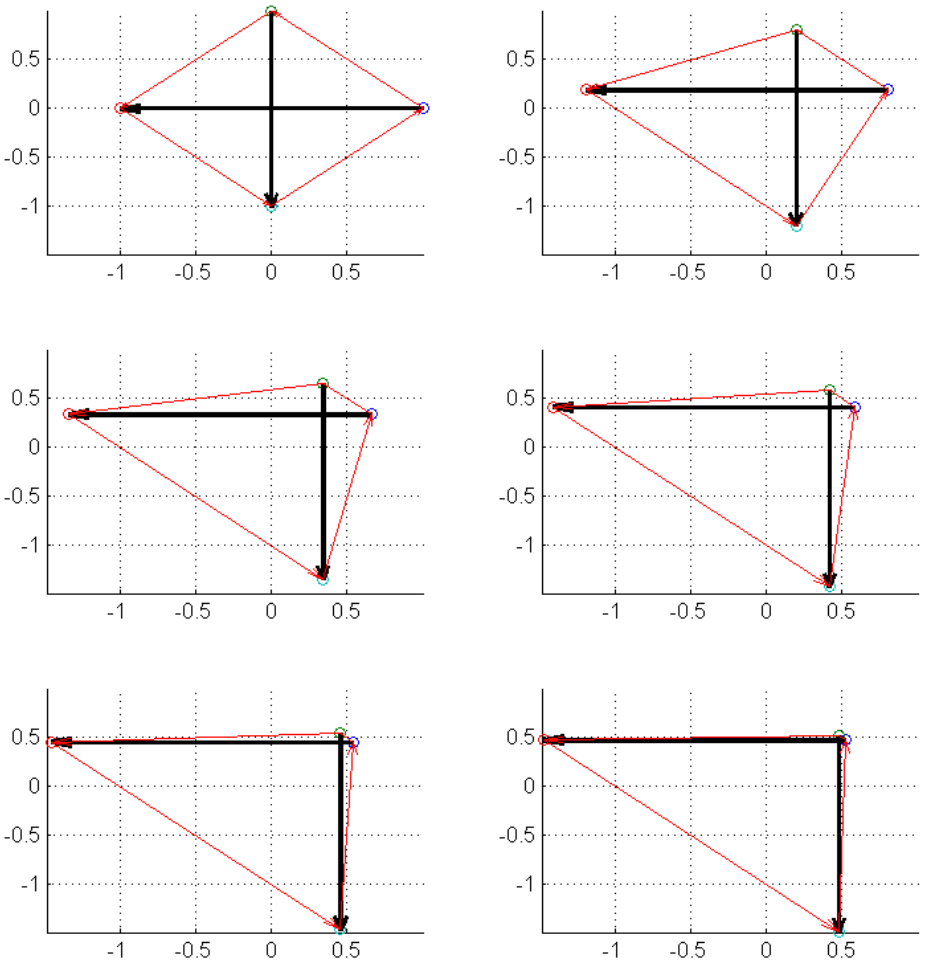

Figure 8. 2D cross transformation time-lapse for control case 3

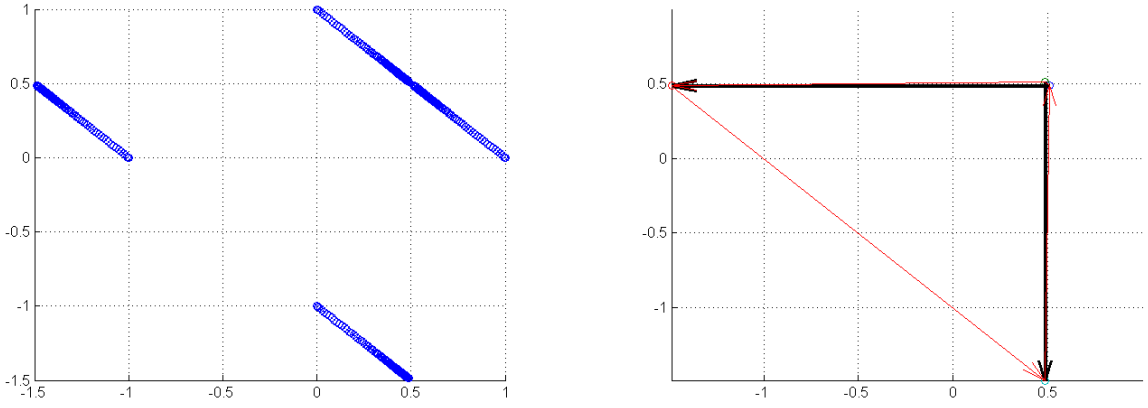

a. Node history b. Final member positions

Figure 9. 2D cross node history and final member position for control case 3

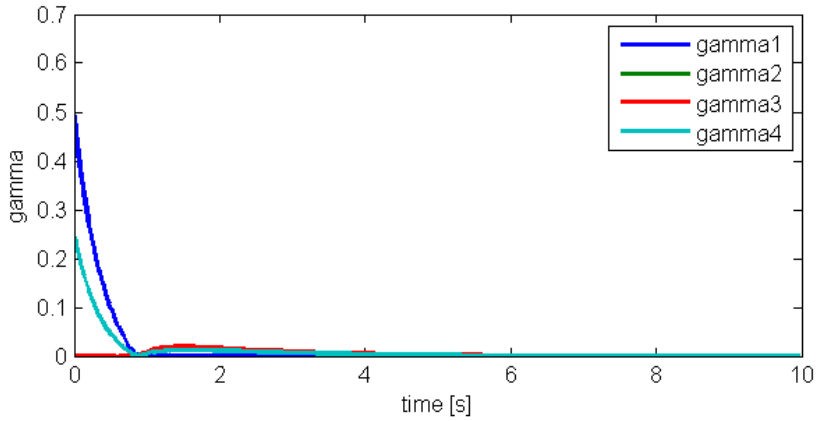

Figure 10. 2D cross tension history for control case 3

B. 3D Prism

To demonstrate how the developed control method scales up to more complex structures, a few cases are assessed involving a simple 3D tensegrity prism. This simple triangular prism is a standard test case for testing tensegrity dynamics in three dimensions. It consists of three bars and nine strings and is defined by the following connectivity and initial node matrices. The initial configuration of the 3D prism system is shown in Figure 11.

$$C = \begin{bmatrix} -1 & 1 & 0 & 0 & 0 & 0 \\ 0 & -1 & 1 & 0 & 0 & 0 \\ 1 & 0 & -1 & 0 & 0 & 0 \\ 0 & 0 & 0 & -1 & 1 & 0 \\ 0 & 0 & 0 & 0 & -1 & 1 \\ 0 & 0 & 0 & 1 & 0 & -1 \\ -1 & 0 & 0 & 1 & 0 & 0 \\ 0 & -1 & 0 & 0 & 1 & 0 \\ 0 & 0 & -1 & 0 & 0 & 1 \\ -1 & 0 & 0 & 0 & 1 & 0 \\ 0 & -1 & 0 & 0 & 0 & 1 \\ 0 & 0 & -1 & 1 & 0 & 0 \end{bmatrix}$$

$$N_0 = \begin{bmatrix} 1.0 & 0.5 & 0 & 1.0 & 0.5 & 0 \\ 0 & 0.87 & 0 & 0 & 0.87 & 0 \\ 0 & 0 & 0 & 1 & 1 & 1 \end{bmatrix}$$

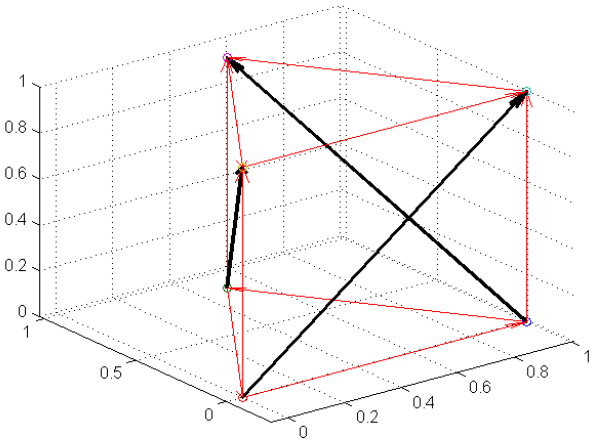

Figure 11. Initial configuration of 3D prism

Case 1: All nodes to x=0, y=0

The given case for the 3D prism involves moving all nodes to $x = 0$ and $y = 0$. This is partly motivated by the concept of deployable and collapsible structures—in this case, the goal is to solve for the tension histories required to collapse the prism down to its most compact configuration. The shape objective matrices for this task are as follows:

$$L = \begin{bmatrix} 1 & 0 & 0 \\ 0 & 1 & 0 \end{bmatrix} \tag{76}$$

$$R = \begin{bmatrix} 1 & 0 & 0 & 0 & 0 & 0 \\ 0 & 1 & 0 & 0 & 0 & 0 \\ 0 & 0 & 1 & 0 & 0 & 0 \\ 0 & 0 & 0 & 1 & 0 & 0 \\ 0 & 0 & 0 & 0 & 1 & 0 \\ 0 & 0 & 0 & 0 & 0 & 1 \end{bmatrix} \tag{77}$$

$$\bar{Y} = \begin{bmatrix} 0 & 0 & 0 & 0 & 0 & 0 \\ 0 & 0 & 0 & 0 & 0 & 0 \end{bmatrix} \tag{78}$$

A 6-image time-lapse of the resulting transformation is given in Figure 12, the node position history and final structure configurations are shown in Figure 13, and tension histories for the transformation are shown in Figure 14. Intuitively, this desired final configuration seems physically achievable, and the obtained results concur.

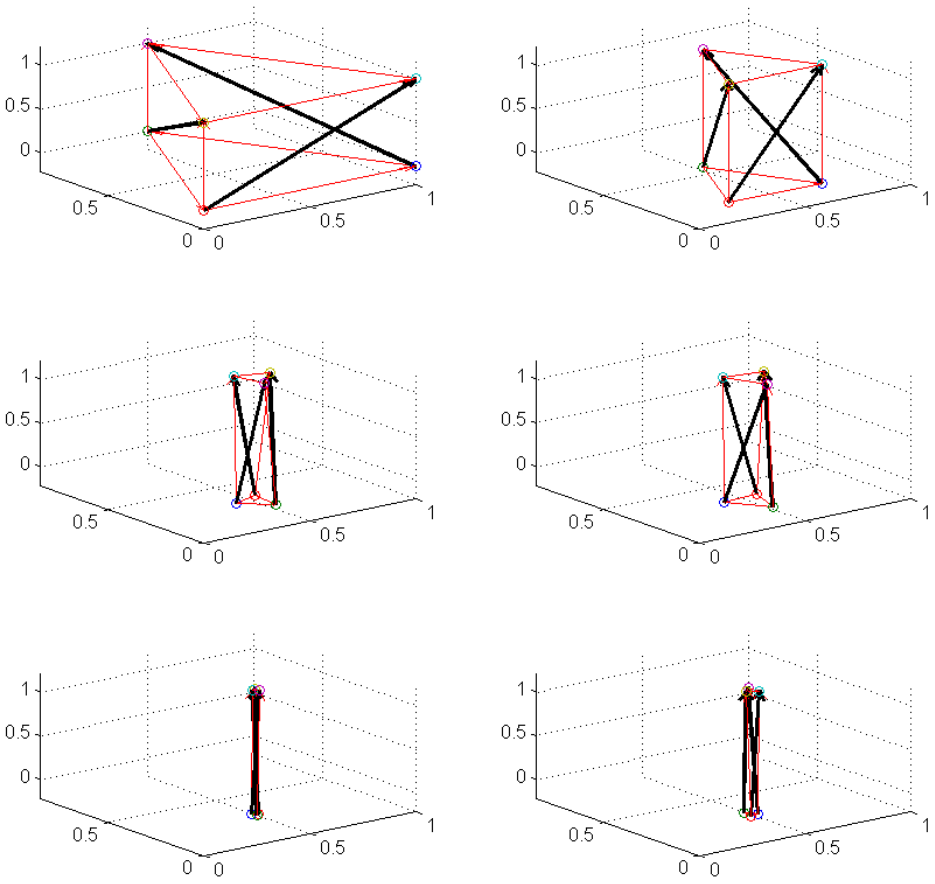

Figure 12. 3D prism transformation time-lapse for control case 1

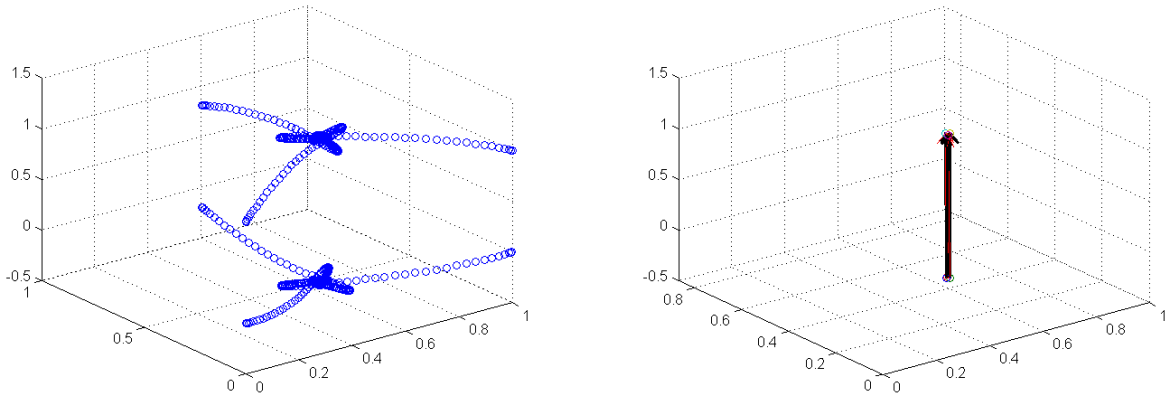

a. Node history b. Final member positions

Figure 13. 3D prism node history and final member position for control case 1

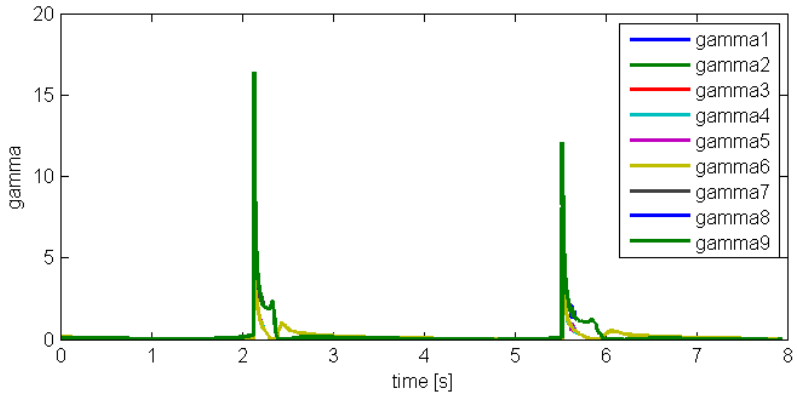

Figure 14. 3D prism tension history for control case 1

Case 2: Nodes 1, 2, and 3 remain at initial x and y positions, and nodes 4, 5, and 6 go to x=0.5, y=0.2887

As a second example of driving multiple nodes to multiple positions, this second case for the 3D prism involves keeping nodes 1, 2, and 3 at their initial x and y positions while simultaneously driving nodes 4, 5, and 6 to $x = 0.5$, $y = 0.2887$. Essentially, the intent here is to transform the triangular prism into a pyramid. The shape objective matrices for this task are found to be:

$$L = \begin{bmatrix} 1 & 0 & 0 \\ 0 & 1 & 0 \end{bmatrix} \tag{79}$$

$$R = \begin{bmatrix} 1 & 0 & 0 & 0 & 0 & 0 \\ 0 & 1 & 0 & 0 & 0 & 0 \\ 0 & 0 & 1 & 0 & 0 & 0 \\ 0 & 0 & 0 & 1 & 0 & 0 \\ 0 & 0 & 0 & 0 & 1 & 0 \\ 0 & 0 & 0 & 0 & 0 & 1 \end{bmatrix} \tag{80}$$

$$\bar{Y} = \begin{bmatrix} 1 & 0.5 & 0 & 0.5 & 0.5 & 0.5 \\ 0 & 0.866 & 0 & 0.2887 & 0.2887 & 0.2887 \end{bmatrix} \tag{81}$$

A 6-image time-lapse of the resulting transformation is given in Figure 15, the node position history and final structure configurations are shown in Figure 16, and tension histories for the transformation are shown in Figure 17. Once again, a solution is found for the desired shape change, which agrees with intuition.

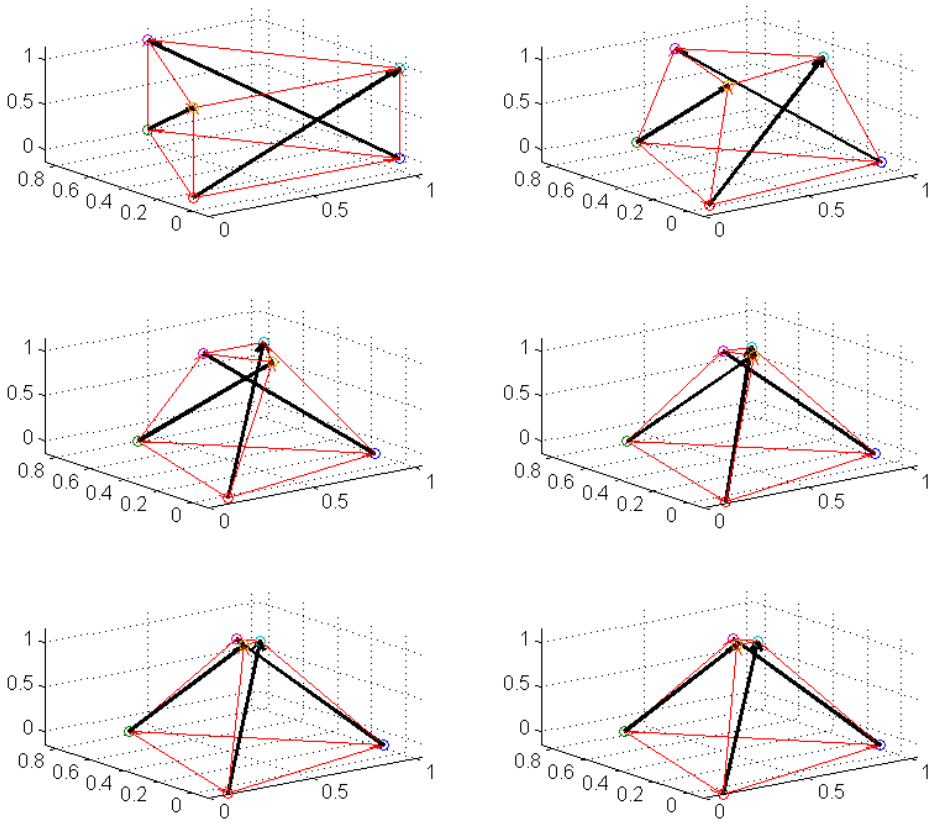

Figure 15. 3D prism transformation time-lapse for control case 2

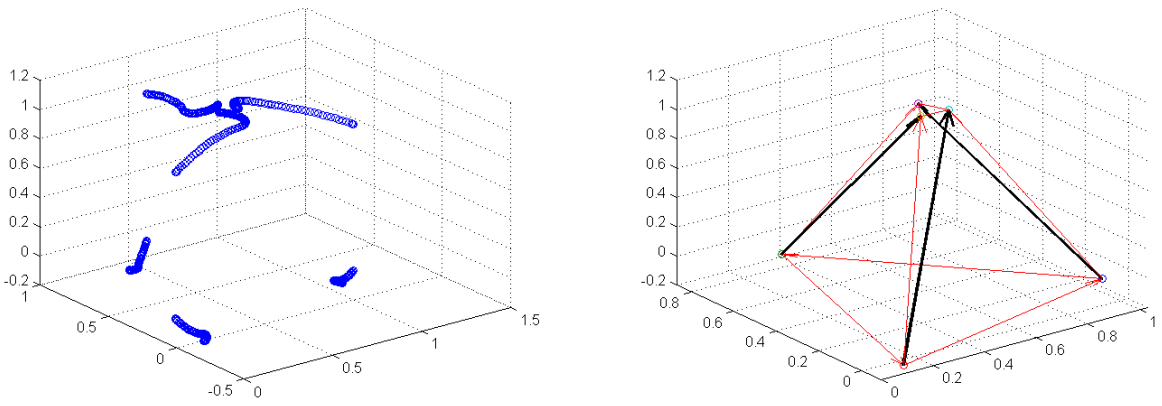

a. Node history

b. Final member positions

Figure 16. 3D prism node history and final member position for control case 2

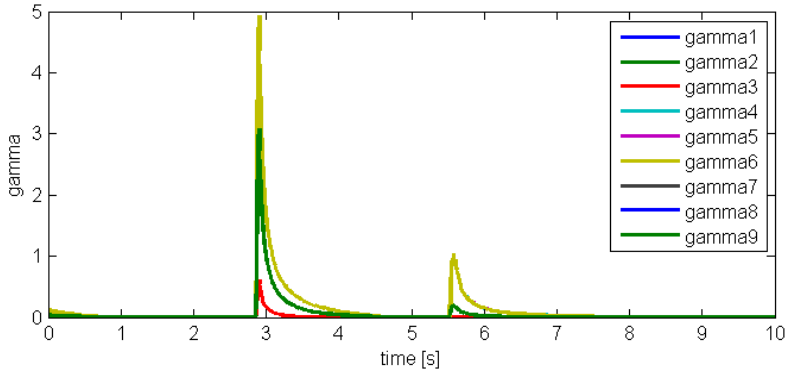

Figure 17. 3D prism tension history for control case 2

VI. Conclusions

In this work, a novel approach to tensegrity shape control was developed and demonstrated. Based on the presented results, the following conclusions are drawn:

1. The developed control law is capable of driving the nodes of Class 1 tensegrity structures to desired positions through changes in string tensions.
2. The developed shape control method successfully scaled from a 6-member structure to a 12-member structure without modification.
3. Transformation solutions for specified shape objectives can be found with a positivity constraint on tensions.

VII. Future Work

This work lays a foundation for the greater goal of fully achieving tensegrity shape control. While results have been presented here with and without tension positivity constraints for two simple systems, a great deal of future work is required before this method can be experimentally demonstrated.

1. **Assess scalability with more complex structures.** Although the control law scaled without issue between a 6-member and 12-member structure, further analysis is required in assessing overall scalability.
2. **Identify necessary conditions for control.** As mentioned, one intuitively expects there to exist structure configuration and shape objective combinations that are unsolvable. Rather than relying on trial and error to avoid such combinations, necessary conditions for control must be formally defined.
3. **Account for structure self-interference.** The results presented in this work do not account for interference between structural members. That is, using the described tensegrity definitions and dynamics, both bars and strings are allowed to freely intersect and pass through one another. This will need to be addressed before any transformation solution is deemed to be physically realizable.
4. **Include external forces and disturbances.** Structures, at least metaphorically, do not exist in a vacuum. External forces will always be experienced by any given structure. For a transformation solution to be physically realizable, simulation needs to demonstrate stability in the face of these external disturbances.

The above tasks represent the various short-term extensions of this work, but there exist many other possible avenues of future development. Potential areas of long-term development include coupling shape controllability and mass minimization in tensegrity structure design, applying optimal control methods to the task of

shape control, and demonstrating the capability of tensegrity shape control with specific morphing structure applications.

References

[1]Cornel Sultan and Robert Skelton. Deployment of tensegrity structures. *International Journal of Solids and Structures*, 40(18):4637–4657, 2003.

[2]Cornel Sultan and Robert E Skelton. Tendon control deployment of tensegrity structures. In *5th Annual International Symposium on Smart Structures and Materials*, pages 455–466. International Society for Optics and Photonics, 1998.

[3]Maurıcio C de Oliveira, Robert E Skelton, and Waileung Chan. Minimum mass design of tensegrity towers and plates. In *Decision and control, 2006 45th IEEE conference on*, pages 2314–2319. IEEE, 2006.

[4]Robert E Skelton and Mauricio C de Oliveira. *Tensegrity Systems*, volume 1. Springer, 2009.

[5]Robert E Skelton, F Fraternali, G Carpentieri, and A Micheletti. Minimum mass design of tensegrity bridges with parametric architecture and multiscale complexity. *Mechanics Research Communications*, 58:124–132, 2014.

[6]Hiroshi Furuya. Concept of deployable tensegrity structures in space applications. *International Journal of Space Structures*, 7(2):143–151, 1992.

[7]Gunnar Tibert. *Deployable Tensegrity Structures for Space Applications*. Royal Institute of Technology, 2002.

[8]AG Tibert and S Pellegrino. Deployable tensegrity reflectors for small satellites. *Journal of Spacecraft and Rockets*, 39(5):701–709, 2002.

[9]S Djouadi, R Motro, JC Pons, and B Crosnier. Active control of tensegrity systems. *Journal of Aerospace Engineering*, 11(2):37–44, 1998.

[10]Cornel Sultan, Martin Corless, and Robert E Skelton. Peak-to-peak control of an adaptive tensegrity space telescope. In *1999 Symposium on Smart Structures and Materials*, pages 190–201. International Society for Optics and Photonics, 1999.

[11]Chao Zhao, Chuang Li, and Nan Zhou. A deployable telescope imaging system with coilable tensegrity structure for microsatellite application. In *ISPDI 2013-Fifth International Symposium on Photoelectronic Detection and Imaging*, pages 89081B–89081B. International Society for Optics and Photonics, 2013.

[12]Jeroen Van de Wijdeven and Bram De Jager. Shape change of tensegrity structures: Design and control. In *American Control Conference, 2005. Proceedings of the 2005*, pages 2522–2527. IEEE, 2005.

[13]Narongsak Kanchanasaratool and Darrell Williamson. Modelling and control of class nsp tensegrity structures. *International Journal of Control*, 75(2):123–139, 2002.

[14]Chandana Paul, Francisco J Valero-Cuevas, and Hod Lipson. Design and control of tensegrity robots for locomotion. *Robotics, IEEE Transactions on*, 22(5):944–957, 2006.

[15]Jack B Aldrich and Robert E Skelton. Control/structure optimization approach for minimum-time reconfiguration of tensegrity systems. In *Smart Structures and Materials*, pages 448–459. International Society for Optics and Photonics, 2003.

[16]Anders S Wroldsen, Maurício C De Oliveira, and Robert E Skelton. A discussion on control of tensegrity systems. In *Decision and Control, 2006 45th IEEE Conference on*, pages 2307–2313. IEEE, 2006.

[17]AS Wroldsen, MC De Oliveira, and RE Skelton. Modelling and control of non-minimal non-linear realisations of tensegrity systems. *International Journal of Control*, 82(3):389–407, 2009.

[18]Robert E Skelton. Dynamics and control of tensegrity systems. In *IUTAM Symposium on Vibration Control of Nonlinear Mechanisms and Structures*, pages 309–318. Springer, 2005.